Available online at www.sciencedirect.com
SCIENCE DIRECT®
Optics Communications 214 (2002) 65–75
OPTICS COMMUNICATIONS
www.elsevier.com/locate/optcom

Linearly constraint color pattern recognition with a non-zero order joint transform correlator

Chih-Sung Wu, Chulung Chen *, Jian-Shuen Fang

Department of Electrical Engineering, Yuan Ze University, Taoyuan 320, Taiwan

Received 11 February 2002; received in revised form 20 May 2002; accepted 25 July 2002

Abstract

In this paper, we purpose a multi-channel single-output non-zero order JTC (NOJTC) to achieve linearly constraint optimization on output correlation energy. The system can be carried out by the power-spectrum subtraction strategy and the design of an ideal reference function with the technique of Lagrange multipliers. Once the zero-order part is removed, the desired correlation peaks are found to be quite distinctive and sharp. The correlator also shows the advantage of distortion invariance and good detection ability.

PACS: 42.30.Sy; 42.79.Hp

Keywords: Joint transform correlator; Color pattern recognition

1. Introduction

The joint transform correlator (JTC) proposed by Weaver and Goodman [1] is interesting in optical pattern recognition since it has many advantages (e.g., less alignment requirement and less system complexity) over some more conventional filters such as the 4-*f* VanderLugt system [2]. In common with conventional correlators, operations performed by JTCs are shift-invariant. Nevertheless, the conventional JTCs (CJTCs) suffer from large correlation sidelobes, large autocorrelation bandwidth, low light efficiency and poor discrimination ability. These handicaps are practically due to the existence of the zero-order power spectrum, which also hinders applications to multi-target detection. Therefore, numerous efforts have been made to improve the JTC performance. To alleviate this drawback, Lu and coworkers [3,4] presented a non-zero order JTC (NOJTC) with a phase-shifting technique by which the output diffraction and input spatial domain can more efficiently be utilized. Some zero-order removal methods have also been proposed and demonstrated [5,6]. For distortion-invariant pattern recognition with JTCs, Alam et al. [7] introduced a fringe-adjusted joint transform correlator based

* Corresponding author. Tel.: +886-3-463-8800x426; fax: +886-3-463-9355.
E-mail address: chulung@saturn.yzu.edu.tw (C. Chen).

0030-4018/02/$ - see front matter
PII: S0030-4018(02)02129-6

on the Newton–Raphson algorithm. However, there is no theoretical guarantee that this algorithm will converge to a solution. Recently, Chen et al. [8,9] used the method of Lagrange multipliers to design a reference function that can produce sharp correlation peaks.

In most cases, VanderLugt correlators and JTCs are implemented to deal with monochromatic images. In reality, most of the visual signals are composed of color information, which drives the development of color pattern recognition [10–12]. On the other hand, the concept of multi-channel JTC has been proposed in the literature [13,14]. For color pattern recognition, the multi-channel JTC system has been implemented by spatial separation of the spectrum for each color channel at the Fourier plane with arranged objects located at the input plane. Deutsch et al. [15] demonstrated a multi-channel single-output JTC by the arrangement of elements for all color channels at the input plane. Unfortunately, their concept led to enormous zero-order part composed of six auto-correlation terms that result in poor detection efficiency.

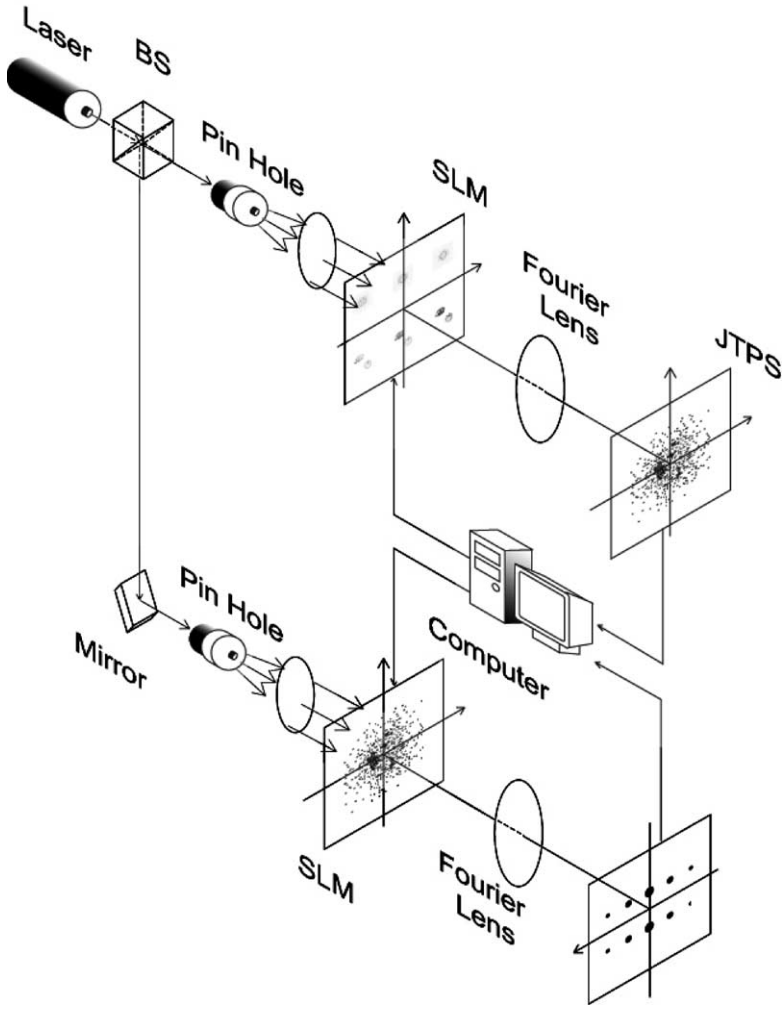

Fig. 1. Optoelectronic implementation of a multi-channel single-output NOJTC for color pattern recognition.

In this paper, we purpose a linearly constraint optimization method for performing color pattern recognition with the multi-channel NOJTC, which has many advantages over other monochromatic or conventional systems. We tested the correlator with rotated and noisy target images. The proposed correlator is found to have better discriminant ability for the test target.

2. Analysis

The basic concept of our JTC system is based on Yu's scheme [16]. The architecture of a JTC consisting of two spatial light modulators (SLMs) is shown in Fig. 1. A coherent laser beam illuminates the first spatial light modulator (SLM) comprising the joint images at the input plane, which is in fact the front focal plane of the first Fourier lens. Diffraction propagation from the SLM results in the Fourier transform operation. A CCD camera placed at the back focal plane of the first Fourier lens is utilized to capture the joint transform power spectrum (JTPS), which is the modulus square of Fourier transform of the input scene. Subsequently, the JTPS subtraction strategy is applied to remove the zero-order term. A computer performs the removal procedure here. The subtracted JTPS is then transferred through the computer to the second SLM for the inverse Fourier transform. At last, the correlation output without zero-order term can be obtained at the back focal plane of the second Fourier lens.

To analyze it mathematically, the input object to the JTC is assumed to be

$$f(x,y)=\sum_{i=1}^{N_c}[r_i(x-x_i,y-y_0)+t_i(x-x_i,y+y_0)], \tag{1}$$

where N_c is the channel number, $r_i(x,y)$ is the component of the reference image, and $t_i(x,y)$ is the component of the test image at the input plane. The separations between the reference channel and the corresponding target channel are the same.

A color image can be treated as the combination of a red color image, a green color image, and a blue color image. Therefore, the reference and test image can be separated into red, green, blue channels, respectively. In this case, N_c turns out to be 3, and the input joint image contains six grayscale patterns. Fig. 2(a) shows one arrangement of these six grayscale images in the input. Three grayscale images corresponding to the red, green, and blue channels (r_1 or r_R, r_2 or r_G, r_3 or r_B) of the reference image are placed in the upper part of the input joint image. Another three grayscale images corresponding to the red, green, and blue components (t_1 or t_r, t_2 or t_g, t_3 or t_b) of the color test image are placed in the lower part of the input

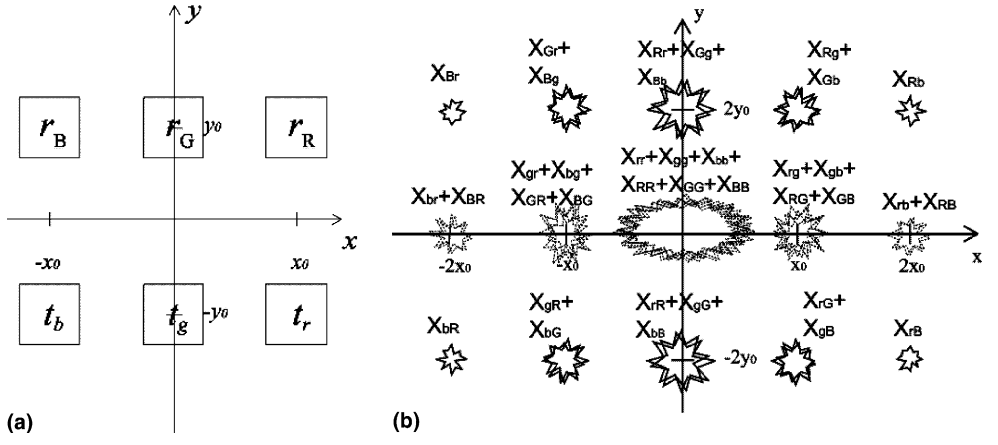

Fig. 2. (a) Arrangement of six grayscale images from the red, green, and blue components of the reference and test image at the input plane. (b) Locations of the correlation distribution at the output plane. The capital letter in a correlation term refers to the color component of the reference image; the lowercase letter represents the corresponding color component of the input test image.

joint image. After the application of the Fourier transform operation, the corresponding JTPS can be formulated as

$$\begin{aligned}|F(u,v)|^2 &= \left|\sum_{i=1}^{3} R_i(u,v)\exp[-j(ux_i+vy_0)]\right. \\ &\quad \left.+\sum_{m=1}^{3} T_m(u,v)\exp[-j(ux_m-vy_0)]\right|^2 \\ &= \left|\sum_{i=1}^{3} R_i(u,v)\exp[-j(ux_i+vy_0)]\right|^2 \\ &\quad +\left|\sum_{m=1}^{3} T_m(u,v)\exp[-j(ux_m-vy_0)]\right|^2 \\ &\quad +\sum_{i=1}^{3}\sum_{m=1}^{3} R_i^*(u,v)T_m(u,v) \\ &\quad \times\exp[ju(x_i-x_m)+j2vy_0] \\ &\quad +\sum_{i=1}^{3}\sum_{m=1}^{3} T_m^*(u,v)R_i(u,v) \\ &\quad \times\exp[-ju(x_i-x_m)-j2vy_0], \end{aligned} \tag{2}$$

where the asterisk * indicates the complex conjugate, (u,v) is the spatial angular frequency coordinate of the joint-spectrum plane, $R_i(u,v)$ and $T_m(u,v)$ represent, respectively, the Fourier transforms of $r_i(x,y)$ and $t_m(x,y)$.

A strong zero-order term will be produced in each channel due to the inherent nature of the JTC. To remove all the zero-order terms, the JTPS subtraction strategy [17] can be utilized. However, a generalized zero-order spectrum removal procedure can be done as follows:

1. Display the grayscale images for the red, green, and blue components of the input scene only. Capture the power spectrum, and store it in the computer.
2. Display the grayscale images for the red, green, and blue components of the reference only. Capture the power spectrum, and store it in the computer.
3. Send the captured JTPS to the computer for the zero-order removal.
4. Subtract the recorded JTPS by the power spectra captured in step 1 and step 2, and obtain the non-zero order JTPS (NOJTPS).
5. Send the NOJTPS to the SLM and acquire the final correlation at the output plane.

Thus, the NOJTPS is

$$\begin{aligned}\text{NOJTPS} &= \sum_{i=1}^{3}\sum_{m=1}^{3} R_i^*(u,v)T_m(u,v) \\ &\quad \times\exp[ju(x_i-x_m)+j2vy_0] \\ &\quad +\sum_{i=1}^{3}\sum_{m=1}^{3} T_m^*(u,v)R_i(u,v) \\ &\quad \times\exp[-ju(x_i-x_m)-j2vy_0]. \end{aligned} \tag{3}$$

After the application of the Fourier transform operation, the field distribution at the output plane can be written as

$$\begin{aligned}\mathrm{O}(x,y) &= \sum_{i=1}^{3}\sum_{m=1}^{3} X_{im}(-x,-y) \\ &\quad \otimes\delta(x-x_i+x_m,y-2y_0) \\ &\quad +\sum_{i=1}^{3}\sum_{m=1}^{3} X_{im}^*(x,y) \\ &\quad \otimes\delta(x+x_i-x_m,y+2y_0), \end{aligned} \tag{4}$$

where $\otimes$ denotes the convolution operation, and the correlation between $r_i(x,y)$ and $t_m(x,y)$ is defined as

$$\begin{aligned}X_{im}(x,y) &= r_i(x,y)\circ t_m(x,y) \\ &= \int\int r_i^*(x',y')(x+x',y+y')\mathrm{d}x'\,\mathrm{d}y'. \end{aligned} \tag{5}$$

We can see that the zero-order term is removed. The correlation peak intensity distribution produced at the output plane is shown in Fig. 2(b). The subscripts in capital letters and lowercase letters denote the input reference and target image, respectively. For example, X_{Rr} represents the correlation peak between r_{R} and t_{r}.

The coherent addition of all three cross-correlation peaks between the input target and the reference image for all color channels will take place at $(0,2y_0)$ and $(0,-2y_0)$. In fact, Eq. (4) can be expressed as

$$\begin{aligned}\mathrm{O}(x,y) &= \sum_{i=1}^{3}\left[X_{ii}(-x,-y)\otimes\delta(x,y-2y_0)\right. \\ &\quad \left.+X_{ii}^*(x,y)\otimes\delta(x,y+2y_0)\right]+\text{o.t.}, \end{aligned} \tag{6}$$

where o.t. represents other terms.

One important objective in pattern recognition is to detect the target with different geometric

distortion, e.g., rotation and scaling, etc. To achieve this goal and to reduce correlation sidelobe energy, we can minimize the average correlation energy of all training images while keeping the desired correlation peaks at a specified height. Similar technique for the monochromatic case can be found in the literature [8,18].

For the multi-channel color pattern recognition, let H_k be the Fourier transform of h_k, where $k = \mathrm{R}, \mathrm{G}, \mathrm{B}$. To minimize the average correlation energy for all training images in each channel, we assume that there are N centered training target images spanning the expected distortion-invariant feature set. Let g_{kn} denote the color component of the nth training image with d pixels present at the input plane. Hence, $h_k \otimes g_{kn}$ and $H_k^* G_{kn}$ form a Fourier transform pair. Because of the symmetry of the output distribution, the values of the correlation intensity at positions $(0, 2y_0)$ and $(0, -2y_0)$ are identical. The complex amplitude value of one correlation peak is

$$C_{kn}(0,0) = \int\int H_k^*(u,v) G_{kn}(u,v)\,\mathrm{d}u\,\mathrm{d}v, \quad n = 1,2,\ldots,N. \tag{7}$$

In discrete form, Eq. (7) can be rewritten in matrix or vector notation as follows:

$$\hat{M}_k^{\mathrm{T}} \hat{H}_k^* = [C_{k1}(0,0) C_{k2}(0,0) \cdots C_{kN}(0,0)]^{\mathrm{T}} = \hat{P}_k, \tag{8}$$

where $\hat{M}_k$ is a $\boldsymbol{d} \times \boldsymbol{N}$ matrix in which each column vector is obtained by sampling $M_{kn}(u,v)$ from the left to the right and from the top to the bottom; similar process for $H_k(u,v)$ leads to a column vector $\hat{H}_k$; the superscript T stands for the transpose operator of a matrix; $\hat{P}_k$ is the correlation peak requirement vector of size N with $C_{kn}(0,0)$ as entries, which can be specified by the user as the same constant to yield equal correlation peaks in response to all training images.

By applying Parseval's theorem, which states the law of the conservation of energy between the space domain and Fourier frequency domain, the cross-correlation energy in either half-output plane for each training image would be

$$\int\int |C_{kn}(x,y)|^2 \mathrm{d}x\,\mathrm{d}y = \int\int H_k(u,v) |M_{kn}(u,v)|^2 H_k^*(u,v)\,\mathrm{d}u\,\mathrm{d}v, \quad n = 1,2,\ldots,N. \tag{9}$$

In the same way, Eq. (9) leads to the average cross-correlation energy function as follows:

$$E_k = \hat{H}_k^{\mathrm{T}} \hat{D}_k \hat{H}_k^*, \quad k = \mathrm{R}, \mathrm{G}, \mathrm{B}, \tag{10}$$

where $\hat{D}_k$ is a real-valued diagonal matrix of size $\boldsymbol{d} \times \boldsymbol{d}$; d is the total pixel number; each diagonal entry is given by calculating $\sum_{n=1}^{N} |M_{kn}(u,v)|^2 / N$.

With the help of Lagrange multipliers [8], the solution to the minimization of the average cross-correlation energy given in Eq. (10) while satisfying the constraints in Eq. (8) for each channel is

$$\hat{H}_k = \hat{D}_k^{-1} \hat{M}_k \left[\hat{M}_k^{+} \hat{D}_k^{-1} \hat{M}_k \right]^{-1} \hat{P}_k^*, \quad k = \mathrm{R}, \mathrm{G}, \mathrm{B}, \tag{11}$$

where the superscript + denotes the conjugate transpose.

The inversion of $\hat{D}_k$ is simple since it is a diagonal matrix. Moreover, $\hat{M}_k^{+} \hat{D}_k^{-1} \hat{M}_k$ is of size $N \times N$, its inversion is not complicated. Therefore, the computation of $\hat{H}_k$ is not difficult.

The solution in Eq. (11) is a vector representation in the frequency domain. As the column vector $\hat{H}_k$ is rearranged as a square matrix H_k, the final optimum reference function in the input domain can be obtained by the inverse Fourier transform on $H_k(u,v)$; that is,

$$h_k(x,y) = \Im^{-1}\{H_k(u,v)\}, \quad k = \mathrm{R}, \mathrm{G}, \mathrm{B}, \tag{12}$$

where $\Im^{-1}$ denotes the inverse Fourier transform.

To examine the detection ability, the system must yield a sharp correlation peak. In fact, one of the important aspects in pattern recognition must be the accuracy of detection, which can be determined by the sharpness of the correlation profiles. The peak response is defined to be the intensity of the maximum correlation peak occurring at the output plane

$$P = \max_{x,y} \{|C(x,y)|^2\} = |C(x_M, y_M)|^2, \tag{13}$$

where $C(x,y)$ is the correlation output, and (X_M, Y_M) denotes the peak position.

The sharpness of the correlation peak can be measured with the peak to correlation energy (PCE) ratio at the desired area, which is defined as

$$\mathrm{PCE} = \frac{P}{\int\int |C(x,y)|^2 \,\mathrm{d}x\,\mathrm{d}y}. \tag{14}$$

Thus, we see that the sharper the correlation profile is, the higher the accuracy of target detection.

The other important aspect in pattern recognition is the detection ability, which can be defined as the peak to sidelobe ratio (PSR) at the desired area, as given by

$$\mathrm{PSR} = \frac{P}{\max\limits_{x,y\in\Omega}\{|C(x,y)|^2\}}, \tag{15}$$

where $\Omega = \{(x,y)||x - x_M| > 2, |y - y_M| > 2\}$.

In the above equation, the sidelobe (or the secondary peak) is defined to be the highest intensity point in the correlation plane at points at least two pixels away from the correlation peak P. In other words, the higher the peak-to-sidelobe ratio is, the higher the pattern detection ability.

Basically, a color image provides more information than a monochromatic one, and therefore color information could contribute somehow to a better correlation performance. We assume that g_{kn} is the color component of the nth training image, g_n is the grayscale transformation of the color training image, G_n is the Fourier transform of g_n, and H is the synthesized reference function (in Fourier domain) from all G_n. It is hoped that the PCE of the multi-channel NOJTC is greater than that of the single-channel monochromatic NOJTC. This condition can be formulated as follows:

$$\frac{\left|\sum_{k=1}^{3}\int\int H_k^*(u,v)G_{kn}(u,v)\mathrm{d}u\,\mathrm{d}v\right|^2}{\int\int\left|\sum_{k=1}^{3}H_k^*(u,v)G_{kn}(u,v)\right|^2\mathrm{d}u\,\mathrm{d}v} > \frac{\left|\int\int H_k^*(u,v)G_{kn}(u,v)\mathrm{d}u\,\mathrm{d}v\right|^2}{\int\int\left|\sum_{k=1}^{3}H_k^*(u,v)G_{kn}(u,v)\right|^2\mathrm{d}u\,\mathrm{d}v}. \tag{16}$$

3. Numerical results

In the system of the electronic correlator, high-speed digital signal processors can perform a 512×512 point Fourier transform (using the FFT algorithm) in 100 ms. The Fourier transform approach can be dramatically improved by using a hybrid electro-optic processor. A SLM developed by Boulder Nonlinear Systems can support 512×512 2D optical Fourier transforms at frame rates of over 1000 Hz. The Fourier transform can be performed at the speed of light as soon as the operands are present, regardless of the number of pixels in the SLM or detector. This advantage is due to the inherent parallelism of the system: since the whole image goes through the Fourier transform lens simultaneously, all of the output points are created at the same time. An optical 2D Fourier transform takes a few nanoseconds (the time needed for the light to transverse the system). The speed of the system is only limited by the rate at which the data can be input to the spatial light modulator and read by the CCD array.

The performance of the multi-channel single-output system is studied by the Matlab software package. The joint input image consists of two parts: the upper part contains the red, green, blue components from the synthesized reference image, and the lower part involves the corresponding color components from the input target scene. First, we introduce the noise-free input image in the multi-channel single-output NOJTC for comparison. In pattern recognition process, images can be affected by various kinds of degradation. Hence, input images with various kinds of noise will be examined next. Furthermore, the capability of distortion invariance is our study of interest, and is verified in the third part of the simulation. Finally, the PCE and PSR values with respect to various numbers of training images to design the reference image will be illustrated.

In the subsequent simulation, initially, we have selected 36 color images for the training set (see Fig. 3), which is assumed to be descriptive of all distorted target images (later we use 360). Therefore, there are 36 training images for each channel to construct the associated reference function. To

Fig. 3. Original color images for the training set.

avoid overlapping of the correlation distribution in this case, all target images and reference images in the input scene consist of 64×64 pixels while the vertical and horizontal intervals are chosen to be 128 and 64 pixels, respectively. The synthesis of the reference image and the electronic transfer of JTPS can be achieved by computer. Hence, the running time is machine-dependent. The transfer of JTPS can be improved by designing a special interface with parallel processing capability. The synthesis of these 3 reference images from 360 color training images took 2 min on a 1 GHz PC. It can be done before the correlation process goes on.

3.1. Result for a noise-free input image

The target object in this paper is chosen to be a color image from a lady beetle. The joint input image is composed of three channels, in the order of red, green and blue, from the right to the left. The upper part of each channel contains the associated reference image, while the lower part includes the corresponding input scene [see Fig. 4(a)]. The overall size of the input image is of 384×384 pixels.

From the preceding analysis, two regions of interest at the output plane are the areas around $(0, -2y_0)$ and $(0, 2y_0)$. The region of interest consists of the coherent addition of overlapping channel correlations. The correlation result shown in Fig. 4(b) illustrates that the correlator successfully detects the target and completely rejects the non-target. Fig. 4(c) is the corresponding 3D plot. All peaks in the graph of correlation intensity have been normalized according to the desired peaks for the reason of observation. Besides two desired peaks, there are few insignificant peaks, which are due to other cross-correlation terms.

According to our numerical analysis of output spectra in color pattern recognition with CJTCs, where the input scene is the same as in Fig. 4(a),

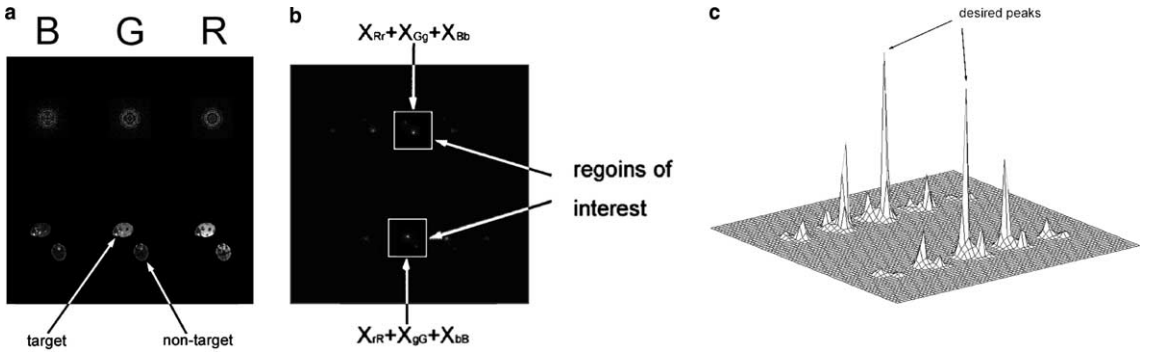

Fig. 4. (a) Input plane of an NOJTC (RGB channels from the right to the left) with noise-free test images. (b) Correlation output. White spots in the rectangles are the desired correlation terms. The subscript letter denotes the associated color composition. (c) 3D profile. One can clearly tell the desired parts from others.

the zero-order peak can be about 3700 times higher than the desired ones [see Fig. 5(a) and (b)]. An experiment under such a condition makes observation very difficult. Therefore, by applying extra steps in the JTPS subtraction technique, we can make the recognition capability of NOJTCs better than that of CJTCs.

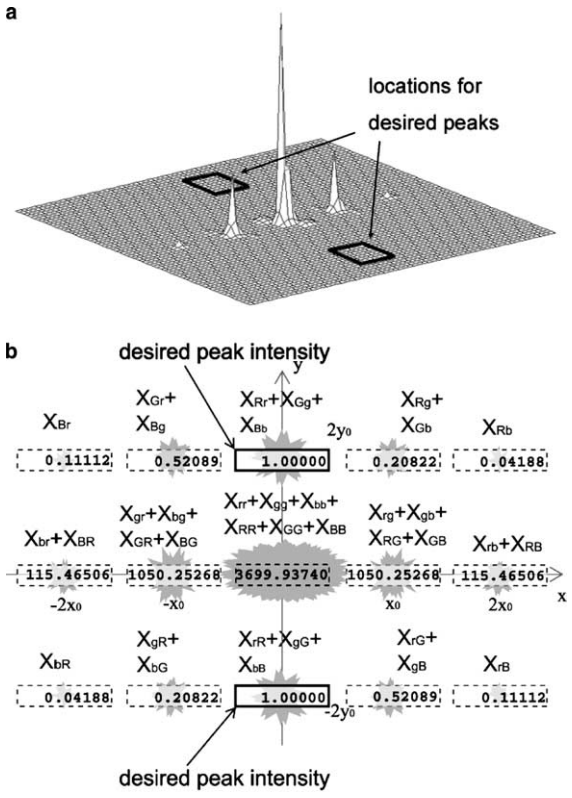

Fig. 5. (a) 3D profile of an NOJTC. (b) The local peak intensity values of overlapping correlations at the output plane of a CJTC. These values have been modified in ratio.

3.2. Results for distorted multiple images and noisy images

To recognize distorted multiple images and noisy images is of some interest in many applications. To see the detection performance of multiple images, Fig. 6(a) depicts the input plane under test. The input image is composed of three objects. One non-target object locates at the bottom left quadrant of the input image and two rotated targets aside. Fig. 6(b) shows the corresponding 3D output plot. The system yields sharp correlation peaks to detect targets and discriminates against non-target.

To further test the noise performance of the correlator, we add some random noise to the input image as shown in Fig. 7(a). In addition, we choose another input image with leaf background, as illustrated in Fig. 8(a). The leaf background is added independently in the base layer of the test image. Besides the noise, the input images are the same as Fig. 4(a). Both of them consist of one target at the top left quadrant and one non-target at the bottom right quadrant. Fig. 7(b) shows 3D profile for the output correlation intensity of Fig. 7(a). The sidelobes increase due to the occurrence of noise energy. However, the target is clearly

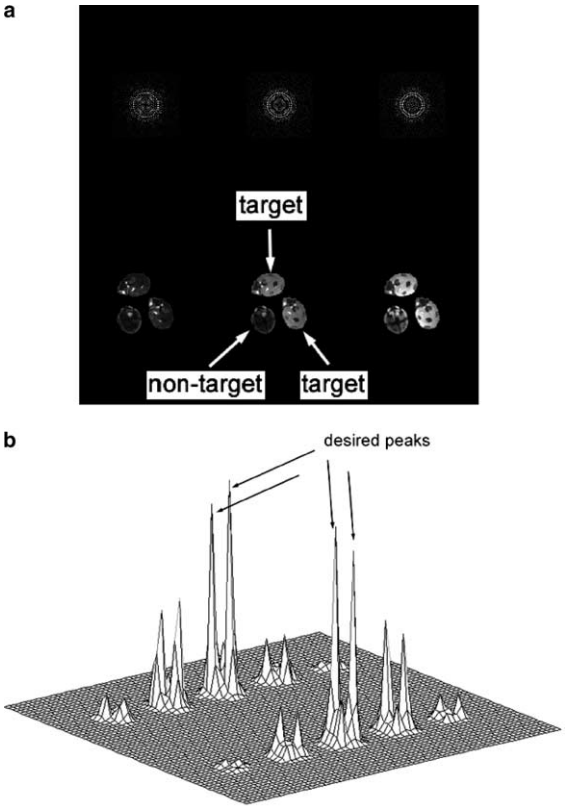

Fig. 6. (a) An input image composed of three objects, two rotated target lady beetles and a beetle from another species. (b) 3D profile for the correlation output. There are four sharp peaks appearing in pairs at the output plane.

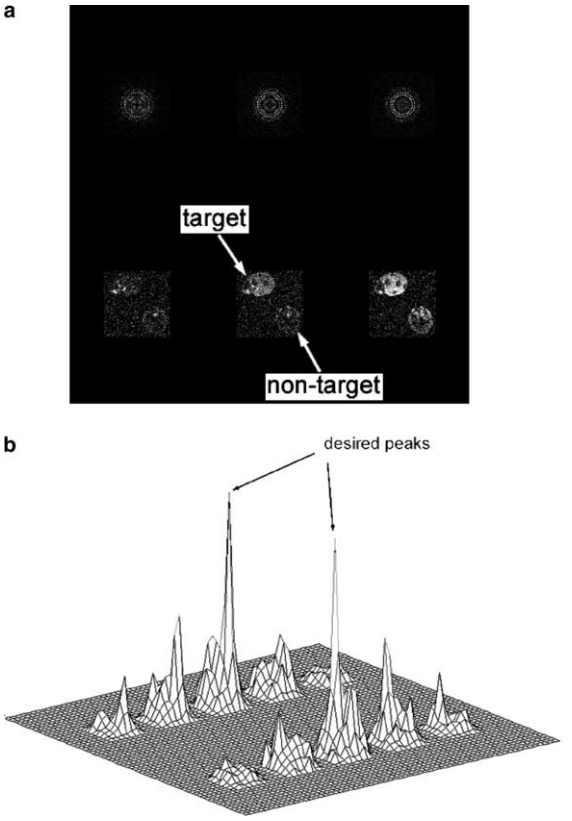

Fig. 7. (a) An input image with overlapping foreground noise. (b) 3D profile for the correlation output.

picked out regardless of the noisy foreground. The corresponding 3D output intensity profile of Fig. 8(a) is plotted in Fig. 8(b). It can be seen that the sidelobes are larger. This is probably because with the increasing energy of the input image, the correlation energy increases. Nevertheless, the desired correlation peaks appear in quite distinguishable shapes, which are good enough to be identified in this case.

3.3. Effect for increasing the number of training set images

The performance of our system depends on many factors; one of them is the number of images in the training set. The more training images we use in the procedure to produce the reference image, the greater recognition capacity the system will be. However, the expansion in the number of training images results in the rise of sidelobes. To clarify the behavior of the monochromatic NOJTC and multi-channel single-output NOJTC, we have plotted the PCE and PSR. Fig. 9 illustrates the PCE with respect to the number of training images to synthesize the reference function for the two cases. On the other hand, the result of PSR analysis is shown in Fig. 10. We obtained these results by generating the reference images from 10 to 360 training images at an increment of 10 images and testing it on the same image shown in Fig. 4(a). As the number of training images increases, the number of constraint equations increases, the ratios decrease due to the increase of the correlation output energy. The PCE ratio is about 30% better than monochromatic NOJTC

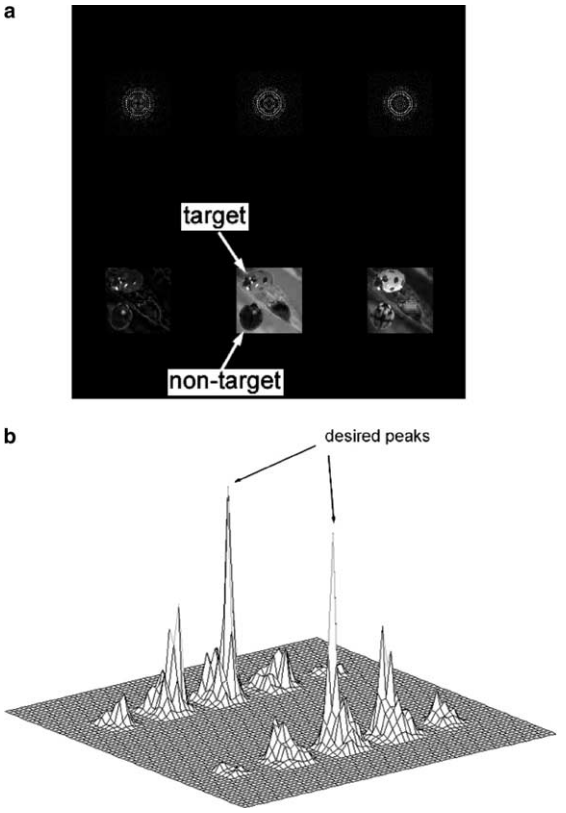

Fig. 8. (a) An input image with leaf background. (b) 3D profile for the correlation output.

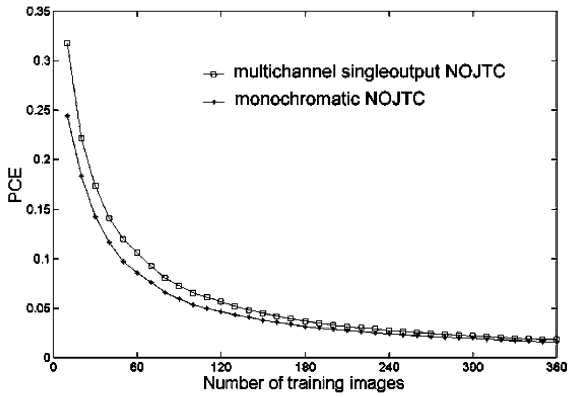

Fig. 9. PCE with respect to the number of training images for different correlators.

for the target under test. The improvement of PSR is, however, not so implicit as PCE. These two figures provide promising results. But if the target has the same reflectance distribution for all three colors, obviously no information is added by using color, the PCE and PSR will be the same as when monochromatic NOJTC is used. In the test, we can see that the multi-channel single-output NOJTC yields slightly better discrimination performance over the tested training images than does the monochromatic NOJTC. We also tested some other objects such as insect and animal images, which are not shown here. Similar results were obtained. However, more targets and theoretical studies have to be investigated to confirm this point.

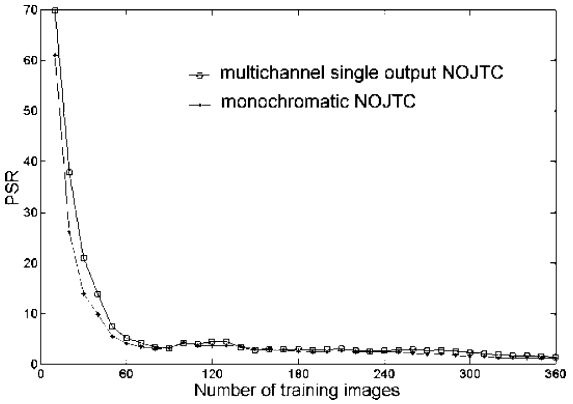

Fig. 10. PSR with respect to the number of training images for different correlators.

4. Conclusion

We have presented an optimization method for multi-channel color pattern recognition with the use of an NOJTC. With prearranged spatial arrangement in the input plane, we can obtain a pair of excellent correlation peaks by superimposing the correlation outputs from each channel of a color image. Theoretically, the system has improved the performance of a JTC in terms of better pixel utilization (as compared to conventional multi-channel JTCs), distortion invariance, higher detection efficiency, possibly good noise tolerance ability, and lower false alarm rate. Moreover, to investigate the performance of recognition capability, the PCE and PSR have been used as metrics in our study.

One of the advantages our system offers is parallel multi-channel processing capability, by which the system can detect targets of different wavelength simultaneously. The proposed system has been demonstrated by the separation of the RGB color channels, but it may be adapted to any multi-channel case. In addition, this system has the benefit of manipulating JTPS to enhance discriminant ability. By eliminating the zero-order part at the output plane, color pattern recognition with an NOJTC could be easier and the system could be smaller as compared to the conventional color JTC setup since the arrangement of input objects could be closer. However, the implementation of multi-channel input images still involves the requirement of a larger SLM and higher cost than single-channel JTC does.

Acknowledgements

The authors would like to thank the reviewers for their constructive criticisms and enlightening suggestions. This research has been supported by the National Science Council, ROC, under Grant No. NSC 90-2215-E-155-006.

References

[1] C.S. Weaver, J.W. Goodman, Appl. Opt. 5 (1966) 1248.
[2] A. VanderLugt, IEEE Trans. Inf. Theory IT-10 (1964) 139.
[3] G. Lu, Z. Zhang, S. Wu, F.T.S. Yu, Appl. Opt. 36 (1997) 470.
[4] F.T.S. Yu, C. Lu, M. Lu, D. Zhao, Appl. Opt. 34 (1995) 1386.
[5] S. Jutamulia, G.M. Storti, D.A. Gregory, J.C. Kirsch, Appl. Opt. 30 (1991) 4173.
[6] S. Jutamulia, D.A. Gregory, Opt. Eng. 37 (1) (1998) 49.
[7] M.S. Alam, X. Chen, M.A. Karim, Appl. Opt. 36 (1997) 7422.
[8] C. Chen, J. Fang, Opt. Commun. 178 (2000) 315.
[9] C. Chen, J. Fang, S. Yin, Microw. Opt. Technol. Lett. 26 (2000) 312.
[10] C. Warde, H.J. Caulfield, F.T.S. Yu, J.E. Ludman, Opt. Commun. 49 (1984) 241.
[11] J.E. Ludman, B. Javidi, F.T.S. Yu, H.J. Caulfield, C. Warde, U. Efron, SPIE Proc. 465 (1984) 143.
[12] F.T.S. Yu, Z. Yang, K. Pan, Appl. Opt. 33 (1994) 2170.
[13] J.H. Feng, G.F. Chin, M.X. Wu, S.H. Yan, Y.B. Yan, Opt. Lett. 20 (1995) 82.
[14] G. Keryer, J.L.B. Tocnaye, Opt. Commun. 118 (1995) 102.
[15] M. Deutsch, J. Garcia, D. Mendlovic, Appl. Opt. 35 (1996) 6976.
[16] F.T.S Yu, X.J. Lu, Opt. Commun. 52 (1984) 10.
[17] C. Li, S. Yin, F.T.S. Yu, Opt. Eng. 37 (1) (1998) 58.
[18] A. Mahalanobis, B.V.K. Vijaya Kumar, D. Casasent, Appl. Opt. 26 (1987) 3633.